



Article

Assessment of the IMERG Early-Run Precipitation Estimates over South American Country of Chile

Luciana das Dores de Jesus da Silva ^{1,*}, Mohammed Mahmoud ², Lisdelys González-Rodríguez ^{3,4}, Safa Mohammed ², Lien Rodríguez-López ⁵ and Mauricio Ivan Aguayo Arias ¹

¹ Facultad de Ciencias Ambientales, Centro Eula, Universidad de Concepción, Concepción 4070386, Chile

² School of Transport and Civil Engineering, Technological University Dublin, D01K822 Dublin, Ireland

³ Facultad de Ingeniería y Negocios, Universidad de las Américas, Sede Concepción, Concepción 4030000, Chile

⁴ Núcleo de Investigación en Data Science (NIDS), Facultad de Ingeniería y Negocios, Universidad de las Américas, Santiago 7500000, Chile

⁵ Facultad de Ingeniería, Arquitectura y Diseño, Lientur 1457, Universidad San Sebastián, Concepción 4070386, Chile

* Correspondence: lucisilva@udec.cl

Abstract: Accurate rainfall measurement is a challenge, especially in regions with diverse climates and complex topography. Thus, knowledge of precipitation patterns requires observational networks with a very high spatial and temporal resolution, which is very difficult to construct in remote areas with complex geological features such as desert areas and mountains, particularly in countries with high topographical variability such as Chile. This study evaluated the performance of the near-real-time Integrated Multi-satellite Retrievals for GPM (IMERG) Early product throughout Chile, a country located in South America between 16°S–66°S latitude. The accuracy of the IMERG Early was assessed at different spatial and temporal scales from 2015 to 2020. Relative Bias (PBIAS), Mean Absolute Error (MAE), and Root-Mean-Squared Error (RMSE) were used to quantify the errors in the satellite estimates, while the Probability of Detection (POD), False Alarm Ratio (FAR), and Critical Success Index (CSI) were used to evaluate product detection accuracy. In addition, the consistency between the satellite estimates and the ground observations was assessed using the Correlation Coefficient (CC). The spatial results show that the IMERG Early had the best performance over the central zone, while the best temporal performance was detected for the yearly precipitation dataset. In addition, as latitude increases, so do errors. Also, the satellite product tends to slightly overestimate the precipitation throughout the country. The results of this study could contribute towards the improvement of the IMERG algorithms and open research opportunities in areas with high latitudes, such as Chile.

Keywords: GPM; IMERG Early; precipitation remote sensing; Chile



Citation: da Silva, L.d.D.J.; Mahmoud, M.; González-Rodríguez, L.; Mohammed, S.; Rodríguez-López, L.; Arias, M.I.A. Assessment of the IMERG Early-Run Precipitation Estimates over South American Country of Chile. *Remote Sens.* **2023**, *15*, 573. <https://doi.org/10.3390/rs15030573>

Academic Editors: Igor Ogashawara and Carmen Cillero

Received: 5 December 2022

Revised: 5 January 2023

Accepted: 10 January 2023

Published: 18 January 2023



Copyright: © 2023 by the authors. Licensee MDPI, Basel, Switzerland. This article is an open access article distributed under the terms and conditions of the Creative Commons Attribution (CC BY) license (<https://creativecommons.org/licenses/by/4.0/>).

1. Introduction

Precipitation is a vital resource of the hydrological cycle [1,2]. Excessive rainfall can lead to a decrease in water quality, which is detrimental to both human health and ecosystem well-being [3,4]. Precipitation measurement is therefore essential for weather forecasting [5]. Rain gauges provide a point measurement that may be used in situations where it is necessary to determine how precipitation is distributed globally [6,7]. However, ground-based measurements are insufficient to cover the spatial and temporal variability of rainfall due to operational and maintenance costs [8–10].

Sectors such as agriculture, hydrology, weather monitoring, numerical forecasting, and climate studies are greatly interested in knowledge of precipitation's spatial and temporal distribution. At this point, we need to go beyond rain gauges for other measuring devices. Radars used to monitor the weather are useful tools for determining how precipitation is distributed throughout their respective coverage areas. Also, satellite precipitation products

provide worldwide coverage and several studies in the field have proved their contribution to science. The development of meteorological satellites in the 1970s made it possible to observe clouds in a hemispheric context. This observation provided the possibility to carry out scientific research in order to advance multiple techniques for detecting meteorological variables remotely.

Remarkably, scientific development to estimate precipitation from radiometric satellites is an ongoing challenge. Among the most widely recognized and currently used precipitation estimates is the Climate Prediction Center Morphing Method (CMORPH) [11–13]. A very popular satellite product devoted to measuring moderate to high rainfall is Multi-Satellite Precipitation Analysis (TMPA, known as 3B42) [14–16]. In addition, other popular precipitation products are widely used, such as Hydroestimator (HYDRO) [16], Precipitation Estimation from Remotely Sensed Information using artificial neural networks (PERSIANN) [17,18], and the new satellite Global Precipitation Measurement (GPM) [10,19,20].

The GPM project is a scientific endeavor that aims to study physics and spatiotemporal variability of the Earth's global precipitation as an essential component of the planet's meteorological, climatological, and hydrological systems [5]. Improved coverage (60°N–60°S) as well as spatial (0.1° × 0.1°) and temporal (30 min.) resolution were all part of the Integrated Multi-satellite Retrievals from GPM (IMERG), in the GPM satellite's mission launch on 27 February 2014. IMERG has three near-real-time rainfall products: Final, Early, and Late [19]. IMERG products have performed well in precipitation research worldwide [20]. For example, in Saudi Arabia, they showed a high correlation between the satellite estimates and the gauge measurements at daily rainfall resolution [19]. However, they showed a moderate correlation performance in Iran [21]. Other studies evaluated the different IMERG products in Iran [22], Finland [10], Greece [23], South America [24], Brazil [25–27], Saudi Arabia [19,28,29], Indonesia [30], Ecuador [31], Pakistan [32] and Chile [15,20,33].

Estimating rainfall in mountainous areas is a challenge, due to the difficulty of establishing a good rainfall station coverage in these areas [28]. Some research has focused on the argument of rainfall coverage versus remote sensing performance in these areas, such as in the Tropical Andes [34], mountainous areas (the Pyrenees) [35], western Alps [36], and Saudi Arabia [32]. These researchers have shown the problems of precipitation detection [34,35] increasing errors in areas exceeding 2000 m elevation [28]. In South America, given the complex topography associated with the Andes Mountains, areas with a significant presence of surface snow and strong spatial contrasts as well as changing precipitation regimes, the uncertainties of IMERG products need to be estimated. Based on research articles, there are uncertainties associated with the satellite estimates, which could be due to factors affecting rainfall estimation, such as the area's hydroclimatic characteristics. In addition to topography, the season of the year influences satellite estimates, reported to result in overestimation or underestimation in most mountainous areas [34–36]. Other potential sources of uncertainty include the scale dependency and the extensive interaction between the dynamics of air circulation and the microphysics of clouds [20]. Because mountainous terrain is often rough and difficult to reach due to its very nature, the use of rain gauges and other remote sensing technologies is frequently constrained by the terrain's characteristics. In many cases, the alternative brings together both of these methodologies, a combination of ground and remote sensing data [29].

In the example of south-central Chile, total rainfall from rain gauges revealed a correlation of 0.66 spatially, between the IMERG Late product and measurements. However, there was a considerable underestimation of rainfall estimated by the satellite identified across the Andes and coastal mountain areas lying at 36.5 degrees south, while the performance was better for northern and valley areas [20]. For the severe event that took place from 28–31 January 2021, Junqueira et al. [25] showed that a correlation of 0.73 was achieved between the gridded IMERG Final product estimates and the gauge measurements. On the other hand, Soto Alvarez et al. [15] analyzed the performance of IMERG Late and Final products for four different macro zones around Chile. No study has been done on the regional and temporal performance of the IMERG Early product over Chile, nor on its

effectiveness in detecting precipitation events across the nation. This is also true of its performance in determining whether major events had taken place. Before putting them to use in any kind of hydrological application, a more comprehensive examination is still required for a better understanding of IMERG product variations, especially in regions with high topographical and climatic variations, such as Chile.

The motivation for this study is therefore:

- The possibility of using these products as a complement or substitute for ungauged and poorly gauged regions;
- A lack of real-time data that can be used for early-warning systems;
- A lack of studies examining the performance of the IMERG Early product in a country or region with a high precipitation variability, such as Chile.

As a result, the primary purpose of this research was to assess the reliability of the IMERG Early product compared to the precipitation data collected from the ground across Chile. This paper's structure is as follows: The research area, data gathering, processing, and statistical measure definitions are all introduced in Section 2. The findings of the study are presented and discussed in Section 3, along with the limitations of the research, including different levels (spatial and temporal). This investigation comes to a close in Section 4, which also contains a conclusion.

2. Datasets and Methodology

2.1. Study Area

Continental Chile is located between 16° and 66° south latitude. Its diversity is due to its vast latitudinal distances (Figure 1a,b). The region has areas with complex topography associated with the Andes Mountains, areas with a significant presence of surface snow and strong spatial contrasts, and low or intense precipitation regimes. It ranges from hyper-arid regions in the north to rainy climates in the extreme south, passing through a climatic transition zone with dry summers and wet winters, whose duration and amount of rainfall increase from north to south. According to the Köppen-Geiger Classification [37], the territory presents five climates: Desert, Mediterranean, Semiarid, Temperate, and Glacial. The arid north occurs from the extreme north, 17.5°S to 30°S, where annual rainfall is around 100 mm. From this latitude, rainfall increases southward, and the wet season increases in duration until at 42°S, with more than 2500 mm per year. It is no longer possible to define a dry summer (Figure 1a). Further south, rainfall continues to increase, reaching up to 5000 mm per year in the insular regions of Aysén and Magallanes. In the altiplano (from 3500 m above sea level), a summer rainfall regime develops, with a maximum of about 400 mm per year. It decreases southward along the peaks until it disappears around 28°S. Rainfall in the central transition region is concentrated in the coldest months. The mountain ranges also affect rainfall distribution; when driven by the wind, the clouds loaded with moisture hit the windward slope, producing heavy rains in this region.

Chile is administratively divided into 16 regions, namely (i) Arica-Parinacota, (ii) Tarapacá, (iii) Antofagasta, (iv) Atacama, (v) Coquimbo, (vi) Valparaíso, (vii) Metropolitana de Santiago, (viii) O'Higgins, (ix) Maule, (x) Ñuble, (xi) Biobío, (xii) Araucanía, (xiii) Los Ríos, (xiv) Los Lagos, (xv) Aysén, and (xvi) Magallanes (see Figure 1a,b and Table 1). These regions were formed based on (<https://www.bcentral.cl/> accessed on 17 January 2022).

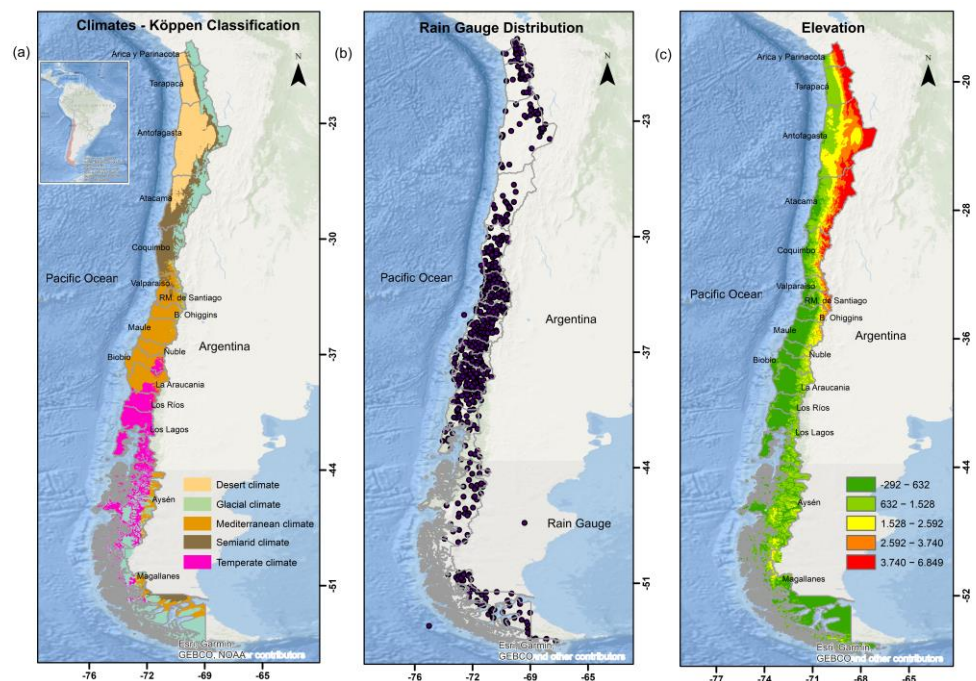


Figure 1. (a) Map of Köppen-Geiger climate classifications by color (based on temperature and precipitation), including political and administrative distribution, (b) location of rainfall gauge stations across Chilean territory, and (c) elevation over Chile. The elevation and distribution of the region were created using an ArcGIS analysis of a shapefile. The shapefiles of Chile and profile elevation were obtained from IDE, <https://www.ide.cl/> (accessed on 4 December 2022) [38].

Table 1. Administrative regions and their rain gauge station.

Administrative Region	Number of Stations	Density per Km	Annual Precipitation
Antofagasta	38	0.0003	100
Araucania	55	0.0017	3000
Arica y Parinacota	27	0.0016	3
Atacama	28	0.0004	250
Aysén	39	0.0004	4266
Biobío	40	0.0017	2000
Coquimbo	65	0.0016	130
Los Lagos	29	0.0006	3514
Los Rios	23	0.0013	3056
Magallanes	66	0.0005	3500
Maule	55	0.0018	792
Metropolitana (RM) de Santiago	43	0.0028	356
Ñuble	28	0.0021	1500
O'Higgins	30	0.0018	739
Tarapacá	23	0.0005	8
Valparaíso	62	0.0038	450

2.2. Data Collection and Processing

2.2.1. Rain Gauge and IMERG Data

Rain gauge data, spanning from 1 January 2015 to 31 December 2020, were downloaded from the Dirección General de Aguas (DGA, <https://snia.mop.gob.cl/>, accessed on 19 January 2022). In this study, a total of 651 rain gauge stations were included and assessed. The stations cover all regions of Chile, as shown in Figure 1b. The following table shows the number of rain gauge stations per region, their density, and the mean annual precipitation.

Daily records, altitude, and ID were collected for 651 rain gauge stations to evaluate rainfall. The station ID provided by the DGA was used to identify the region and a number that refers to the sequence in the database list. A quality check of the daily records data was carried out following Scherrer, S.C. et al. and Estévez, J. et al. [39,40] to detect possible random alterations in the time series. GPM Mission Remote Sensing data were downloaded from NASA (<https://gpm.nasa.gov/>, accessed on 25 January 2022). The IMERG Early product was the focus of this study and was evaluated from 2015 to 2020 (6 years). This product presents near real-time precipitation records at $0.1^\circ \times 0.1^\circ$ resolution every 30 min, totaling 17,520 annual files (17,568 for a leap year).

2.2.2. Data Analysis

To obtain the IMERG precipitation estimates that match the ground measurements, a methodology was adopted from Mahmoud, M.T. et al. [10] which considers the precipitation value within the position of the cell representing the IMERG Early product intersection point against the location coordinates of the precipitation station.

The IMERG Early is provided in an RT-H5 file format, where RT refers to real-time and H5 is an HDF5 file. Following the methodology of Mahmoud, M.T. et al. [19], the precipitation data were extracted just for the country of Chile and converted into an ASCII format. The spatial resolution of the IMERG Early product is 0.1° longitude \times 0.1° latitude. Figure 2 shows the coordinate matching process. The matching process of the coordinates and IMERG Early product files were scripted in MATLAB software following the methodology introduced by previous articles [19,29]. The main steps of the code are: (1) search each rainfall record during each event for the latitude and longitude written in cell position format and ID; (2) read the selected IMERG Early product file and scan the precipitation value within the cell position that represents the GPM intersection point with the location coordinates of the rainfall station; (3) collect the nearest intersection point when that intersection point is located above the quadrilateral of length $0.1^\circ \times 0.1^\circ$ (approximately 11×11 km); and (4) compare rainfall measurements from the specified rainfall station and the selected IMERG Early product intersection. A total of 2192 data files were preprocessed.

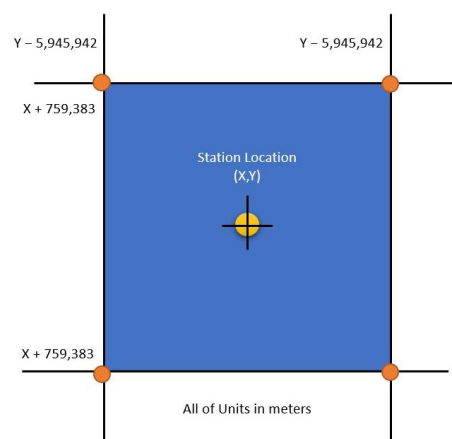


Figure 2. Coordinate Matching as illustrated in Mahmoud, M.T. et al. [10].

2.3. Data Evaluation-Validation Process

Radars cannot be used to directly measure precipitation. Rather, rainfall is calculated based on the amounts measured. Since it is an estimate, it must be validated or checked to ensure its accuracy [10]. Therefore, we require observations from rain gauges so we can evaluate the accuracy of weather radars against satellite rainfall estimates. The IMERG Early product and ground-based precipitation data were put through their paces throughout the validation procedure, which consisted of measuring their performance using six different statistics. These methodologies are further broken down into three categories,

which all apply to different purposes. The first group consists of the mean absolute error (MAE), the root mean squared error (RMSE), and the relative bias (PBIAS) and is used to characterize the biases and inaccuracies that are present within the satellite data when compared to the rain gauge data (Equations (1)–(3)). The second group looks at whether or not the data from the rain gauge and the satellite estimations match up consistently via the use of the correlation coefficient (CC) (Equation (4)). The third group explains the uncertainty surrounding the satellite estimations using three statistical parameters: the false alarm ratio (FAR), the probability of detection (POD), and the critical success index (CSI) (Equations (5)–(7)). All statistical results are shown by boxplot and maps. These metrics are defined as:

$$MAE = \frac{1}{n} \sum_{i=1}^n |S_i - G_i| \quad (1)$$

$$RMSE = \sqrt{\frac{1}{n} \sum_{i=1}^n (S_i - G_i)^2} \quad (2)$$

$$PBIAS = \frac{\frac{1}{n} \sum_{i=1}^n (S_i - G_i)}{\sum_{i=1}^n G_i} \quad (3)$$

$$CC = \frac{\frac{1}{n} \sum_{i=1}^n (S_i - \bar{S})(G_i - \bar{G})}{\sigma_S \sigma_G} \quad (4)$$

$$FAR = \frac{P_s}{P_s + P_{SG}} \quad (5)$$

$$POD = \frac{P_{SG}}{P_{SG} + P_G} \quad (6)$$

$$CSI = \frac{P_{SG}}{P_{SG} + P_s + P_G} \quad (7)$$

3. Results and Discussion

The IMERG Early product accuracy results are presented for the 651 stations evaluated in the Chilean territory. The statistical results are presented in two analyses: spatial and temporal. The topography was also evaluated, including these results in the spatial evaluation session. Some limitations and future remarks are subsequently mentioned.

3.1. Spatial Analysis

3.1.1. Satellite Detection Accuracy

Figure 3 shows the spatial performance for the IMERG Early product using the POD, FAR, and CSI metrics over Chile. The POD, FAR, and CSI indices show that the IMERG Early product performed well in detecting precipitation from the O'Higgins region to the south. The Coquimbo region and the southern regions of Chile showed the highest detection accuracy, with a POD close to 1. On the other hand, the northern regions, mainly the regions of Antofagasta and Atacama, showed low detection accuracy, highlighting the Atacama Desert area for the IMERG Early product. The Rub' al-Khali desert in Saudi Arabia has previously shown low POD and CSI values, demonstrating the satellite's low performance over the desert [19].

In addition, the FAR was calculated to evaluate the false detection from the IMERG Early product. The first seven regions, from Arica and Parinacota to RM de Santiago, presented FAR and CSI values between 0.50–0.90 and 0.00–0.60, respectively, showing poor detections for these regions. Interestingly, there was a gradual reduction of false alarms towards the south, which was consistent with the POD indicator. The FAR results over the Ñuble, Biobío, Araucanía, Los Ríos, and part of the Los Lagos regions showed a decrease, while the CSI values were relatively high. In addition, we could notice that some areas such as the Aysén and Magallanes regions present FAR and CSI values similar to those of the central region. This could be due to the low frequency of pluviometry stations.

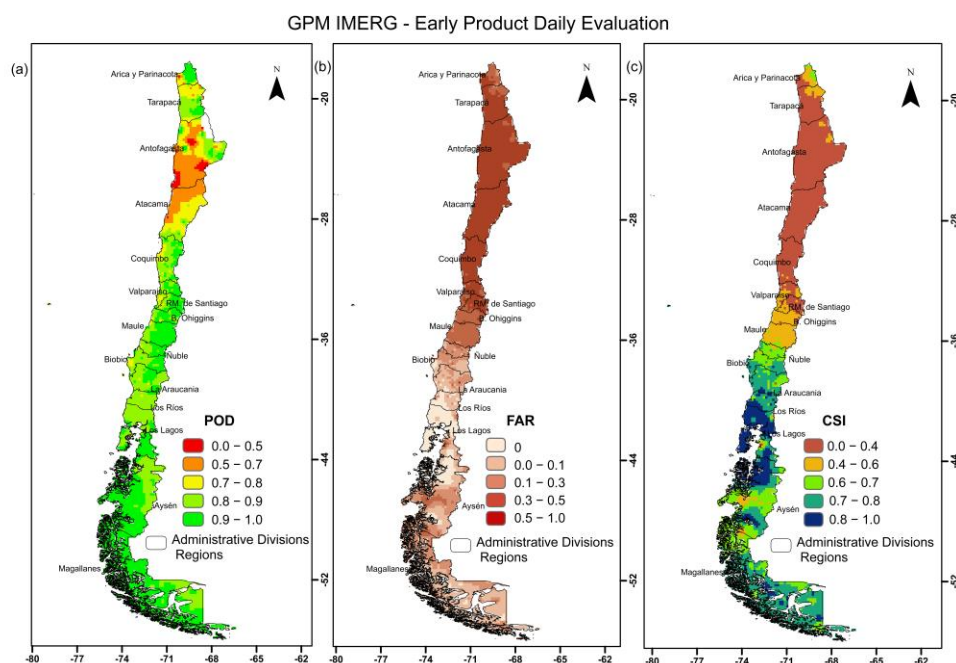


Figure 3. Satellite detection accuracy based on (a) POD, (b) FAR, and (c) CSI.

On the other hand, climatic differences dictate different precipitation regimes. It is notable that there are climatic transition zones throughout the country (see Figure 1a), which have their own characteristics, making it difficult for some precipitation detection [41]. However, Figure 3 shows an improvement in satellite precipitation detection accuracy in Mediterranean and temperate climates (see Figure 1a). Surprisingly reliable values were found for the POD and CSI performance indicators up to 58° S latitude. Similar results have been shown by Mahmoud et al. [10] for high latitudes in Finland using the Early product.

3.1.2. Satellite Error

Boxplots provide the analysis with the degree of dispersion, symmetry, and number of outliers that the statistics present in their daily distribution. Figure 4 shows the errors associated with IMERG Early product satellite precipitation estimates according to RMSE, MAE, and PBIAS. The IMERG Early product displayed a significant error in spatial evaluation precipitation estimation. The RMSE and MAE showed a latitudinal increase until the Los Lagos region. The most noteworthy error was in Los Lagos, with values between 22.34 mm/day and 8.54 mm/day for RMSE and MAE, respectively. Comparing the MAE results reported for the same product in Saudi Arabia, all Chilean regions had a MAE less than 10 mm/day [19]. Therefore, the Early product demonstrates its superiority in the Chilean territory to characterize the biases and inaccuracies present within the satellite data compared to the rain gauge data. The Antofagasta and Atacama regions reported lower mean values of RMSE (2.49 mm/day, 3.19 mm/day) and MAE (0.79 mm/day, 0.45 mm/day), respectively.

The PBIAS estimator revealed a slight precipitation overestimation for all regions. The most significant overestimation detected by the satellite was reported for Arica and Magallanes, with values of 0.14 mm/day. In the case of Arica, this was suggested by the evaporation of precipitation in a drier atmosphere below the cloud base, while in Magallanes, the overestimation could be related to the predominance of snow-covered surfaces, which can be confused with precipitation in the case of algorithms using microwave data [5]. In the case of IMERG, precipitation estimates are given through algorithms that combine observations from microwaves, geostationary sensors, and rain gauges. Other authors have found overestimation results using the IMERG Early product in Iran [22] and Peru [34].

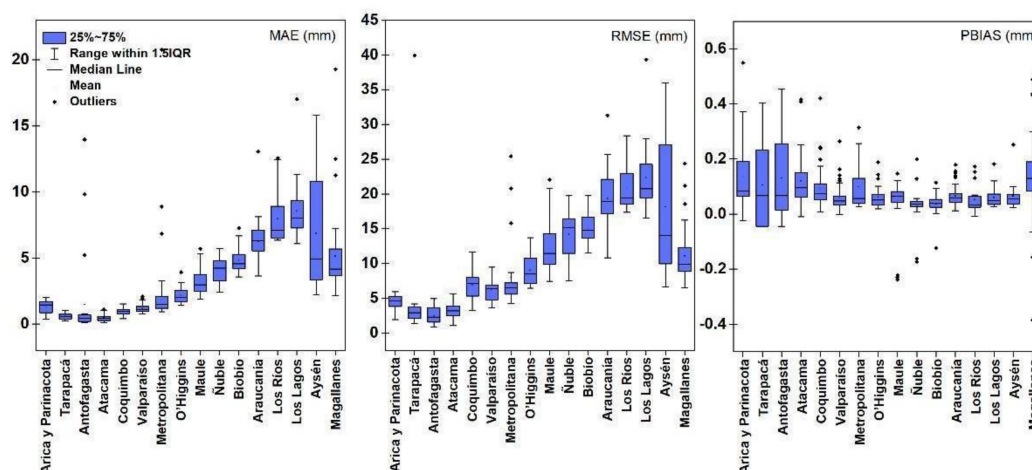


Figure 4. Boxplot of gauge-IMERG Early product errors. 25% and 75% represent the distribution that has an index between the 25th percentile (P25) and 75th percentile (P75), the horizontal line inside the box shows the median, the mean value is included with a black circle, and the so-called “whiskers” mark the maximum and minimum values that are not outside the typical range of the distribution. Outliers are shown with a black diamond.

3.1.3. Topographic Evaluation

Chile is a country with an accentuated topography, with the second largest mountain range in the world, the Andes, among its territory. For this reason, the territory was divided into mountainous (Andes and Coast) and non-mountainous regions (regular terrain zones), and the accuracy of detection in both zones was also measured for the IMERG Early product (see Figures 5 and 6). The spatial assessment indicates that detection accuracy depends on the geological features (topography, land use, and land type). The areas located from latitude 28°S , including coastal mountain, regular terrain areas, and the Andes Mountain range, showed POD values < 0.70 . POD values above 0.9 were found in some Andean mountain range sites, which is much higher than those reported using the IMERG Early product for Saudi Arabia [28]. The lowest POD values are concentrated in the desert region of Chile, where the Atacama Desert is located, which may be related to the low density of stations also present in the area. It should be noted that the interpolation leads to additional uncertainties in pixels without rain gauges than in pixels with them [35]. Therefore, in uncovered areas such as the Atacama Desert, special care must be taken with Early product observations.

From the north to the center, the mountainous and non-mountainous zones show the lowest FAR values (above 0.5). On the contrary, the highest FAR values were recorded from latitude -28°S to the extreme south (-56°S), in high mountain areas and the central continental zone, reaching values between 0.70 and 1.00. From latitude -36°S to the south, optimal FAR and CSI values were found between 0.00–0.30 and 0.60–1.00, respectively. The improvement of POD, FAR, and CSI values from latitude -36°S to the last region (Magallanes) may be related to the fact that the ground-based stations are located at low altitudes (in the case of terrain zones). Therefore, the orographic effect is not included, as these regions are influenced by cold masses and frontal-type precipitation in the wettest seasons (mainly during winter) [42]. The Coastal Mountain range and Andes Mountains range presented the lowest detection accuracy. This might be the result of the very variable terrain (mountainous area) in that section of the nation, which results in a rainfall pattern with high erratic variability. Particularly in the Coastal Mountain range, it may be associated with the fact that, at medium altitudes (600–1200 m) and dominated by the advection of humid maritime air masses, there is an overestimation by the IMERG [35], related to the uncertainties of estimation.

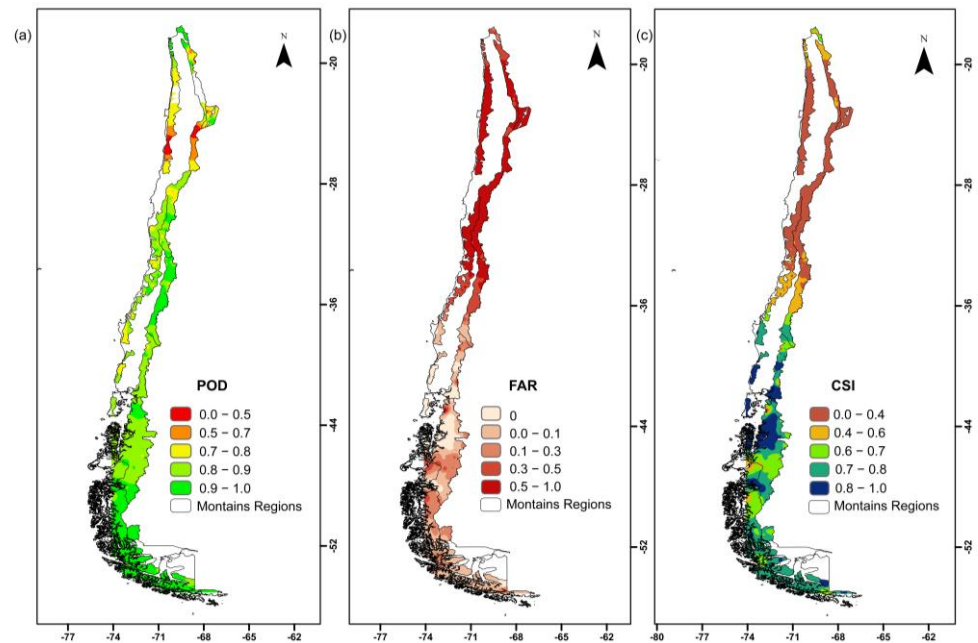


Figure 5. Satellite detection accuracy using (a) POD, (b) FAR, and (c) CSI over mountainous regions.

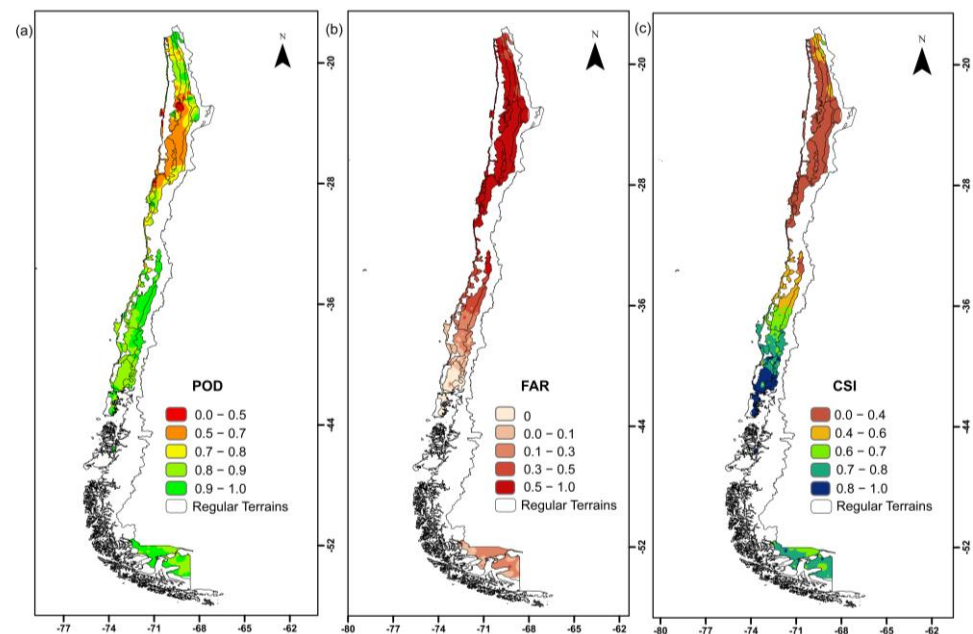


Figure 6. Satellite detection accuracy using (a) POD, (b) FAR, and (c) CSI over the regular terrain's regions.

It is also possible that this is connected to the hilly terrain, which may be difficult to navigate, and the fact that there are fewer surface stations in these regions as in other places and therefore lower detection in the northern region versus the south. Several authors have reported a high error rate in hilly terrain. Navarro et al. [36] indicated that precipitation in the western Alps, Europe, was poorly represented using IMERG. Similar results were found in Saudi Arabia by Mahmoud et al. [28], who found larger errors in coastal, foothill, and high mountain areas when compared to other topographic areas. This research also showed the IMERG Final product's higher accuracy compared to the Early and Late.

3.2. Temporal Analysis

3.2.1. Satellite Detection Accuracy

IMERG Early product performance differences were evaluated for three-time scales: Daily, Monthly, and Yearly. The POD, FAR, and CSI indices were also included (Figures 7–9). Generally, highest detection accuracy was found for the Yearly dataset, while lowest accuracy was observed for the Daily and Monthly datasets. The IMERG Monthly product performed better than the daily goods when compared to rain gauge data.

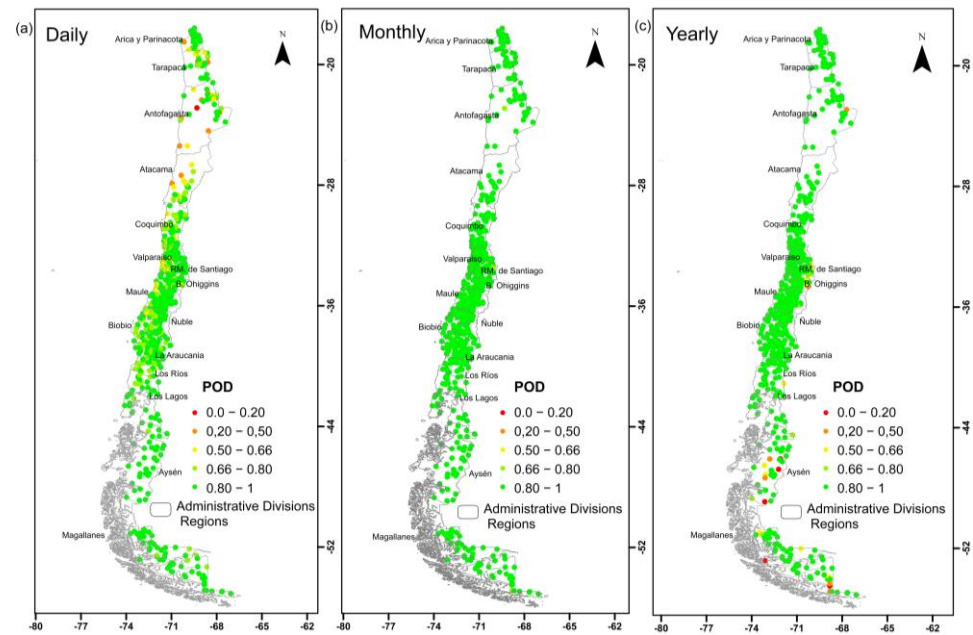


Figure 7. Daily, Monthly, and Yearly POD for IMERG Early product.

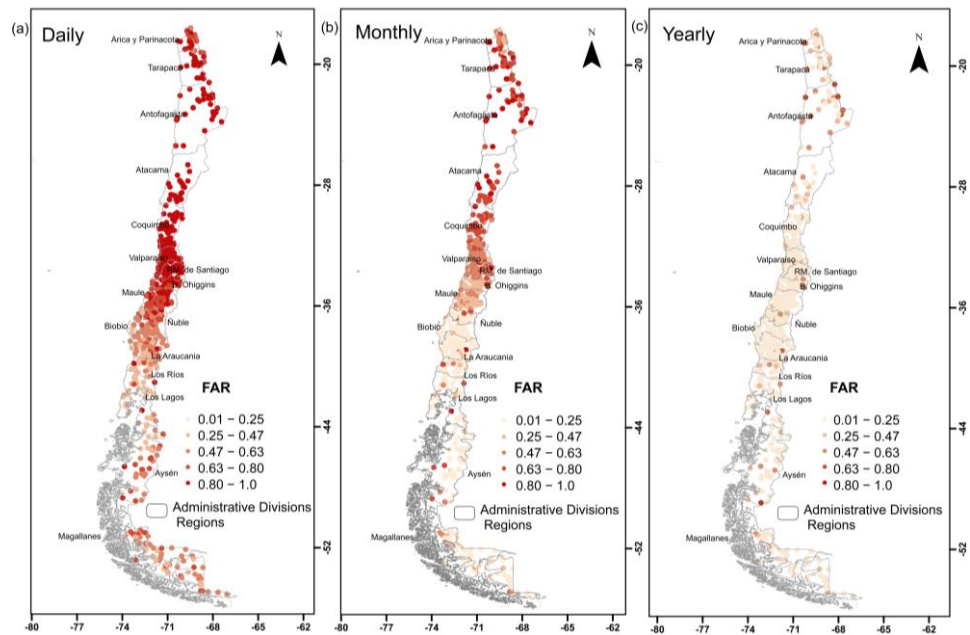


Figure 8. Daily, Monthly, and Yearly FAR for IMERG Early product.

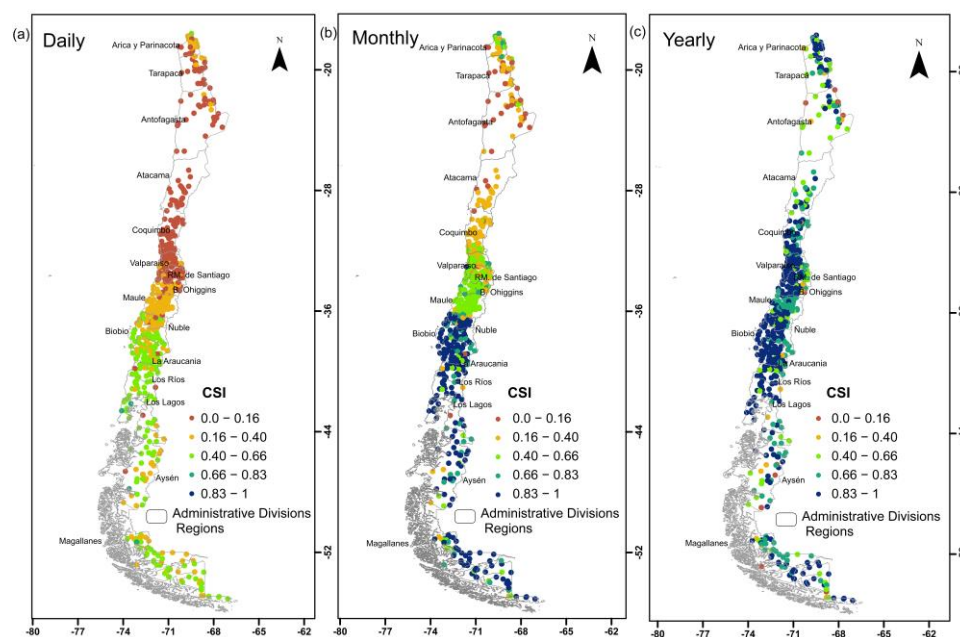


Figure 9. Daily, Monthly, and Yearly CSI for IMERG Early product.

Daily, Monthly, and Yearly POD averages were 0.60, 0.94, and 0.88, respectively. For the Daily resolution, all data have POD values between 0.70 and 1. Each month, the rain gauges recorded POD values between 0.80 and 1. The POD ranged from 0.20 to 1 for the Yearly dataset. Conclusions drawn from POD analyses were corroborated by those drawn from CSI analyses. The FAR findings demonstrate incorrect precipitation detection. For over 70% of gauges, annual FAR values are less than 0.20.

In terms of the false detection of precipitation, the FAR's data brought up several interesting points. The greatest FAR values were obtained from the Yearly and Monthly datasets, with averages of 0.06 and 0.03, respectively. In contrast, numerous erroneous detections were found in the Daily dataset, which had an average FAR value of 0.22. In addition, the Monthly findings suggested that the FAR values can be affected by the aggregation of the data. The erroneous precipitation detections made by the satellite will be obscured if the precipitation data collected at a finer resolution are aggregated into a monthly dataset. There are FAR values of less than 0.47 in both the Daily and Monthly datasets. Nevertheless, it is easy to notice that most of these lower values are centered between the Biobío and Magallanes areas, which are situated in the southern part of Chile.

In this particular instance, the accuracy of precipitation identification was greatest for the Yearly dataset, which averaged 1.0. In the case of the Daily dataset, the satellites precipitations products, demonstrated reasonably good detection accuracy, with an average CSI of more than 0.97 for around 64% of stations, the majority of which span the Ñuble–Magallanes regions. This indicates that these satellites products can cover a wide range of locations. When looking at the Daily dataset, the stations' performance was not very good in the first 12 areas, with CSI values ranging from 0.10 to 0.48. It is important to note the very marked spatial pattern similar to the climatic pattern (see Figure 1a), mainly in the climate transition zones (Valparaíso and RM. de Santiago/Maule–Biobío regions).

3.2.2. Satellite and Rain Gauge Observation Correlation

In Figure 10, the CC was used to evaluate the consistency between rain gauge observations and the IMERG Early product at different time scales. The CC showed significant differences between temporal and spatial scales. The Daily dataset revealed the lowest CC with values below 0.69, followed by the Yearly dataset, which improved CC above 0.69 between the Atacama and Ñuble regions. This was surpassed by the Monthly dataset, which achieved CC values above 0.69 for most stations located between Atacama and

Los Lagos regions, including those stations in the regions of Arica and Parinacota, Aysén, in the mountainous zone. Therefore, the Monthly dataset presented better results than the Yearly and Daily resolutions. This pattern alters towards the central coastal zone, mainly for the Daily database, when decreasing the CC (0.14–0.41). Similar CC results were found by Ramadhan et al. [43] in Indonesia. Among the temporal analyses (Hourly, Daily, and Monthly), poor correlation for IMERG’s Daily data was found versus Monthly data. This could be related to the high variability of rainfall on an IMERG grid, so that a point observation may not be adequate to represent grid rainfall [34].

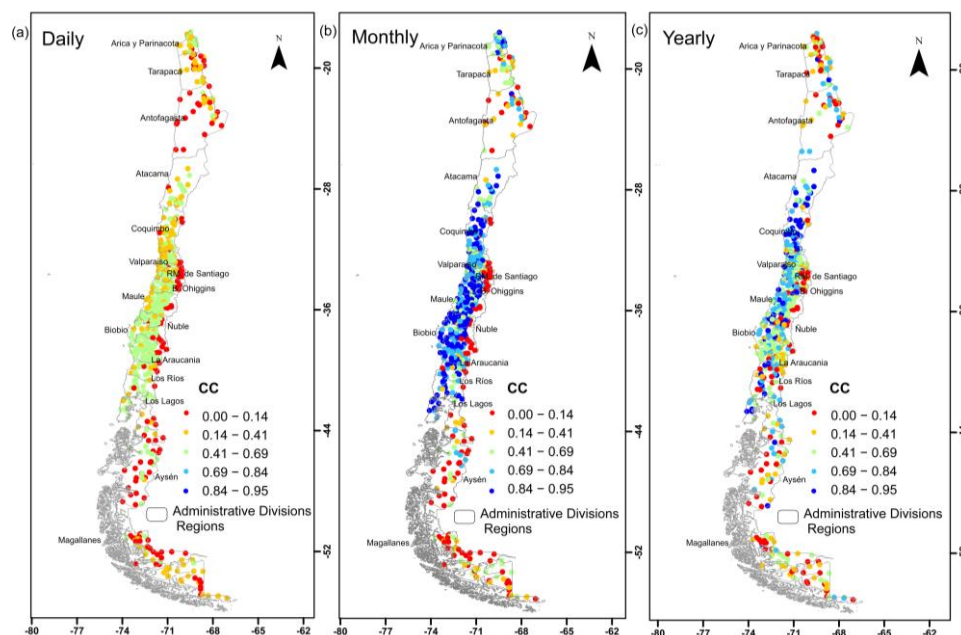


Figure 10. Spatial distributions of CC for the Daily, Monthly, and Yearly resolutions for IMERG Early product.

It is possible to perceive that, for all temporal resolutions, the sectors with low correlation are located in the Andes Mountains, from the Metropolitana de Santiago to Magallanes regions. This may be a consequence of the lower density of pluviometers, heterogeneity of rainfall distribution, or variation in topography [19] across the Chilean territory.

3.2.3. Satellite Error Evaluation

Figure 11a,b compares multiple temporal scales (Monthly and Yearly) using MAE, RMSE, and PBIAS. For Chile, the IMERG Early product showed a significant error in Monthly resolution. The RMSE and MAE showed a latitudinal increase until the Los Lagos region. The most significant error was observed in Los Lagos, with average values of 236.63 mm/month and 165.54 mm/month for RMSE and MAE, respectively. For the Antofagasta and Atacama regions, the lower mean values of RMSE (23.76 mm/month, 25.85 mm/month) and MAE (12.04 mm/month, 11.00 mm/month) were reported. The PBIAS estimator for Monthly and Yearly distributions revealed a slight overestimation for all regions, which found the most significant overestimation for Antofagasta, with values of 0.16 mm/month and 48 mm/year.

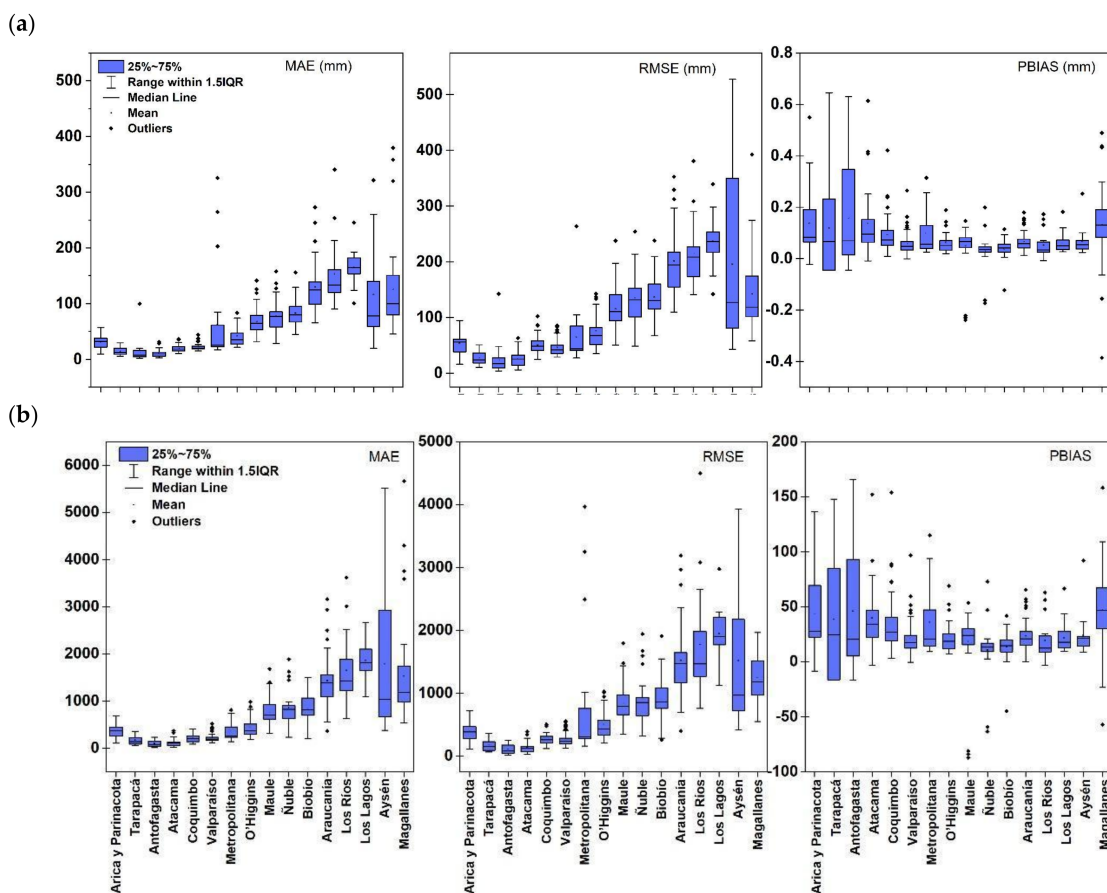


Figure 11. Boxplot of gauge-IMERG Early product for (a) Monthly and (b) Yearly errors. 25% and 75% represent the distribution that has an index between the 25th percentile (P25) and 75th percentile (P75), the horizontal line inside the box shows the median, the mean value is included with a black circle, and the so-called “whiskers” mark the maximum and minimum values that are not outside the typical range of the distribution. Outliers are shown with a black diamond.

Similarly, the Yearly resolution reported increased RMSE and MAE values towards the south. The most significant error was observed in Los Lagos, with average values of 1946.64 mm/year and 1859.49 mm/year for RMSE and MAE, respectively. The IMERG Early product showed a significant error in Daily precipitation estimation for Chile. The RMSE and MAE showed a latitudinal increase until the Los Lagos region. As latitude increases, so does the error, which is justified by the low detection of the sensor in high-latitude areas (above 60°S).

Research on the performance of this satellite precipitation product is necessary, mainly because it offers precipitation estimates at high spatial and temporal resolutions, which is an advantage in non-instrumented areas, as long as the sensor performance is statistically satisfactory. If reliable, this can be used as input data in different types of models for different applications. The GPM product has been recognized for its good performance in various hydrological applications, such as rainfall frequency analysis [44], extreme precipitation [45], flood analysis [46], and drought monitoring [47]. Chile is a country affected by several types of hydrometeorological events [45,48]. As such, we wanted to test the performance of the IMERG Early product to support disaster response and recovery [49]. In addition, there are a limited number of studies consider IMERG Early products in the country. The spatial and temporal resolutions of IMERG provide a valuable product for examining precipitation events [29] that may result in floods, landslides, or other weather-induced phenomena in Chile. However, it is vital to highlight the limitations related to this work.

Several factors can affect detection uncertainty, including errors from ground measurements (instruments, atmospheric conditions, and gaps in the data) and errors from satellite sensors [10,34,35]. Variables such as the brightness of the visible spectrum clouds and cloud error may influence satellite precipitation estimates [50]. It is possible for errors resulting from the use of IMERG algorithms to propagate to applications dependent on IMERG data, like hydrological models [10].

3.3. Limitations and Future Remarks

The general objective of this work has been to assess the performance of the GPM sensor and rainfall stations throughout Chile. The following are some limitations found for this study:

1. Chile's rain gauge network does not have a uniform density for the whole country. The stations are dense in the center of Chile, while in the north and south they are scarce. A dense gauge network would also allow better evaluation, quantifying the errors and uncertainties associated with satellite estimates.
2. Some rainfall stations did not present complete data for the six years evaluated and therefore were not considered in this research.
3. This study considered only the IMERG Early product, since Chile is one of the countries most vulnerable to climate change worldwide. In addition, several hazards are present in the country, including hydrometeorological events. Therefore, measuring the early-warning capability of the sensor for Chile could help in risk management. However, there is a need to carry out a comprehensive study, including Late and Final products.
4. An uncertainty analysis should be carried out to determine whether the El Niño-Southern Oscillation (ENSO) cycle may influence the climate, including precipitation pattern.
5. This study evidences that, despite the technological advances in remote sensing, considerable uncertainties remain in the products from the satellite mission [51,52]. Satellite precipitation estimates are often affected by random and systematic errors (bias). In this case, a systematic error correction approach based on a multiplicative bias correction factor through the ISIMIP [53] or SCALING method [54] will be included in future work.

However, it is possible to add that, despite its limitations, the IMERG Early product reveals a promising path for current and future applications. A possible continuation of this work is to consider an analysis of the IMERG Early product's performance and compare it with other products (Late or Final), considering the type of associated cloudiness [20].

4. Conclusions

This research evaluates the IMERG Early product for the first time, using data from 651 rain gauge stations throughout Chile over the course of six consecutive years. Analysis performed in Chilean territory reveals that hydroclimatic parameters of the zone, rain gauge distribution, and geographic characteristics are most influential in rainfall estimates. The following points conclude the findings of this study:

1. The spatial analysis shows that the IMERG Early product has acceptable detectability for some regions, climates, and reliefs. POD and CSI values indicate that the IMERG Early product is able to detect rain, with better results from the center to the south of the country. However, FAR values are significant in the north of the country (arid region).
2. The Coastal Mountain and Andes Mountains ranges presented the lowest detection accuracy.
3. The worst temporal performance was found for the Daily distribution compared to Monthly and Yearly data. Areas located in the Andes Mountain range showed a lower CC from the Metropolitana de Santiago to the Magallanes regions.
4. For the three temporal distributions (Daily, Monthly, and Yearly), the errors (MAE and RMSE) showed a latitudinal increase and slightly overestimated throughout the country. The PBIAS is higher in the arid region and the Magallanes region.

Overall, this study suggests that the IMERG Early product offers a promising path for current and future applications.

Author Contributions: Conceptualization, L.d.D.d.J.d.S. and L.G.-R.; methodology, L.d.D.d.J.d.S. and M.M.; software, L.d.D.d.J.d.S., L.G.-R. and M.M.; validation, M.M. and S.M.; formal analysis, M.M.; investigation, M.I.A.A.; resources, L.R.-L.; data curation, M.M.; writing—original draft preparation, L.d.D.d.J.d.S., L.G.-R., M.M. and L.R.-L.; writing—review and editing, L.d.D.d.J.d.S., L.G.-R. and M.M.; visualization, L.G.-R. and L.R.-L.; supervision, M.I.A.A.; project administration, M.I.A.A.; funding acquisition, M.I.A.A. All authors have read and agreed to the published version of the manuscript.

Funding: This research was funded by UCO project 1866 at Universidad de Concepción, and Universidad San Sebastian, Chile (UCO project 1866).

Data Availability Statement: Not applicable.

Acknowledgments: L.d.D.d.J.d.S. would like to thank the UCO 1866 project, Universidad de Concepción. Also, L.R.-L. thanks the Universidad San Sebastian, and L.G.-R. gratefully acknowledges the NIDS and Universidad de las Américas, Sede Concepción, Chile.

Conflicts of Interest: The authors declare no conflict of interest.

References

- Levizzani, V.; Cattani, E. Satellite remote sensing of precipitation and the terrestrial water cycle in a changing climate. *Remote Sens.* **2019**, *11*, 2301. [\[CrossRef\]](#)
- D’Odorico, P.; Carr, J.; Dalin, C.; Dell’Angelo, J.; Konar, M.; Laio, F.; Ridolfi, L.; Rosa, L.; Suweis, S.; Tamea, S.; et al. Global virtual water trade and the hydrological cycle: Patterns, drivers, and socio-environmental impacts. *Environ. Res. Lett.* **2019**, *14*, 053001. [\[CrossRef\]](#)
- Dutta, V.; Dubey, D.; Kumar, S. Cleaning the River Ganga: Impact of lockdown on water quality and future implications on river rejuvenation strategies. *Sci. Total Environ.* **2020**, *743*, 140756. [\[CrossRef\]](#) [\[PubMed\]](#)
- Debebe, Y.; Otterpohl, R.; Islam, Z. Remote sensing and multi-criterion analysis for identifying suitable rainwater harvesting areas. *Acta Geophys.* **2022**. [\[CrossRef\]](#)
- Skofronick-Jackson, G.; Kirschbaum, D.; Petersen, W.; Huffman, G.; Kidd, C.; Stocker, E.; Kakar, R. The Global Precipitation Measurement (GPM) mission’s scientific achievements and societal contributions: Reviewing four years of advanced rain and snow observations. *Quart. J. R. Meteorol. Soc.* **2018**, *144*, 27–48. [\[CrossRef\]](#)
- Del Castillo-Velarde, C.; Kumar, S.; Valdivia-Prado, J.M.; Moya-Álvarez, A.S.; Flores-Rojas, J.L.; Villalobos-Puma, E.; Martínez-Castro, D.; Silva-Vidal, Y. Evaluation of GPM Dual-Frequency Precipitation Radar Algorithms to Estimate Drop Size Distribution Parameters, Using Ground-Based Measurement over the Central Andes of Peru. *Earth Syst. Environ.* **2021**, *5*, 597–619. [\[CrossRef\]](#)
- Usovich, B.; Lipiec, J.; Łukowski, M.; Słomiński, J. Improvement of spatial interpolation of precipitation distribution using cokriging incorporating rain-gauge and satellite (SMOS) soil moisture data. *Remote Sens.* **2021**, *13*, 1039. [\[CrossRef\]](#)
- Belete, M.; Deng, J.; Wang, K.; Zhou, M.; Zhu, E.; Shifaw, E.; Bayissa, Y. Evaluation of satellite rainfall products for modeling water yield over the source region of Blue Nile Basin. *Sci. Total Environ.* **2020**, *708*, 134834. [\[CrossRef\]](#)
- Kumar, P.; Debele, S.E.; Sahani, J.; Rawat, N.; Marti-Cardona, B.; Alfieri, S.M.; Basu, B.; Basu, A.S.; Bowyer, P.; Charizopoulos, N.; et al. An overview of monitoring methods for assessing the performance of nature-based solutions against natural hazards. *Earth-Sci. Rev.* **2021**, *217*. [\[CrossRef\]](#)
- Mahmoud, M.T.; Mohammed, S.A.; Hamouda, M.A.; Dal Maso, M.; Mohamed, M.M. Performance of the imerg precipitation products over high-latitudes region of Finland. *Remote Sens.* **2021**, *13*, 2073. [\[CrossRef\]](#)
- Joyce, R.J.; Janowiak, J.E.; Arkin, P.A.; Xie, P. CMORPH: A method that produces global precipitation estimates from passive microwave and infrared data at high spatial and temporal resolution. *J. Hydrometeorol.* **2004**, *5*, 487–503. [\[CrossRef\]](#)
- Liu, J.; Zhang, Y.; Yang, L.; Li, Y. Hydrological Modeling in the Chaohu Lake Basin of China—Driven by Open-Access Gridded Meteorological and Remote Sensing Precipitation Products. *Water* **2022**, *14*, 21. [\[CrossRef\]](#)
- Reddy, N.M.; Saravanan, S. Evaluation of the accuracy of seven gridded satellite precipitation products over the Godavari River basin, India. *Int. J. Environ. Sci. Technol.* **2022**. [\[CrossRef\]](#)
- Noh, G.H.; Ahn, K.H. New gridded rainfall dataset over the Korean peninsula: Gap infilling, reconstruction, and validation. *Int. J. Climatol.* **2022**, *42*, 435–452. [\[CrossRef\]](#)
- Soto-Alvarez, M.; Alcayaga, H.; Alarcon, V.; Caamaño, D.; Palma, S.; Escanilla, R. Evaluation of products 3B42 v7 and 3IMERG for the hydroclimatic regions of Chile. *J. S. Am. Earth Sci.* **2020**, *104*, 102870. [\[CrossRef\]](#)
- Yucel, I.; Kuligowski, R.J.; Gochis, D.J. Evaluating the hydro-estimator satellite rainfall algorithm over a mountainous region. *Int. J. Remote Sens.* **2011**, *32*, 7315–7342. [\[CrossRef\]](#)
- Ingemarsson, I. Retrieving Precipitation over Brazil a Quantile Regression Neural Networks Approach. Master s Thesis, Chalmers University of Technology, Göteborg, Sweden, 2021.

18. Sadeghi, M.; Asanjan, A.A.; Faridzad, M.; Gorooh, V.A.; Nguyen, P.; Hsu, K.; Sorooshian, S.; Braithwaite, D. Evaluation of PERSIANN-CDR constructed using GPCP V2.2 and V2.3 and a comparison with TRMM 3B42 V7 and CPC unified gauge-based analysis in global scale. *Remote Sens.* **2019**, *11*, 2755. [CrossRef]
19. Mahmoud, M.T.; Al-Zahrani, M.A.; Sharif, H.O. Assessment of global precipitation measurement satellite products over Saudi Arabia. *J. Hydrol.* **2018**, *559*, 1–12. [CrossRef]
20. Rojas, Y.; Minder, J.R.; Campbell, L.S.; Massmann, A.; Garreaud, R. Assessment of GPM IMERG satellite precipitation estimation and its dependence on microphysical rain regimes over the mountains of south-central Chile. *Atmos. Res.* **2021**, *253*, 105454. [CrossRef]
21. Sharifi, E.; Steinacker, R.; Saghafian, B. Assessment of GPM-IMERG and other precipitation products against gauge data under different topographic and climatic conditions in Iran: Preliminary results. *Remote Sens.* **2016**, *8*, 135. [CrossRef]
22. Maghsood, F.F.; Hashemi, H.; Hosseini, S.H.; Berndtsson, R. Ground validation of GPM IMERG precipitation products over Iran. *Remote Sens.* **2020**, *12*, 48. [CrossRef]
23. Kazamias, A.P.; Sapountzis, M.; Lagouvardos, K. Evaluation of GPM-IMERG rainfall estimates at multiple temporal and spatial scales over Greece. *Atmos. Res.* **2022**, *269*, 106014. [CrossRef]
24. Palharini, R.S.A.; Vila, D.A.; Rodrigues, D.T.; Quispe, D.P.; Palharini, R.C.; de Siqueira, R.A.; de Sousa Afonso, J.M. Assessment of the extreme precipitation by satellite estimates over South America. *Remote Sens.* **2020**, *12*, 2085. [CrossRef]
25. Junqueira, R.; Viola, M.R.; da S.; Amorim, J.; Camargos, C.; de Mello, C.R. Hydrological modeling using remote sensing precipitation data in a Brazilian savanna basin. *J. S. Am. Earth Sci.* **2022**, *115*, 103773. [CrossRef]
26. Laverde-Barajas, M.; Corzo Perez, G.A.; Dalfré Filho, J.G.; Solomatine, D.P. Assessing the performance of near real-time rainfall products to represent spatiotemporal characteristics of extreme events: Case study of a subtropical catchment in south-eastern Brazil. *Int. J. Remote Sens.* **2018**, *39*, 7568–7586. [CrossRef]
27. da S. Freitas, E.; Coelho, V.H.R.; Xuan, Y.; Melo, D.d.C.D.; Gadelha, A.N.; Santos, E.A.; Galvão, C.d.O.; Ramos Filho, G.M.; Barbosa, L.R.; Huffman, G.J.; et al. The performance of the IMERG satellite-based product in identifying sub-daily rainfall events and their properties. *J. Hydrol.* **2020**, *589*, 125128. [CrossRef]
28. Mahmoud, M.T.; Mohammed, S.A.; Hamouda, M.A.; Mohamed, M.M. Impact of topography and rainfall intensity on the accuracy of imerg precipitation estimates in an arid region. *Remote Sens.* **2021**, *13*, 13. [CrossRef]
29. Mahmoud, M.T.; Hamouda, M.A.; Mohamed, M.M. Spatiotemporal evaluation of the GPM satellite precipitation products over the United Arab Emirates. *Atmos. Res.* **2019**, *219*, 200–212. [CrossRef]
30. Yu, X.; Shi, J.; Feng, L.; Li, C.; Wang, L. A three-dimensional BiOBr/RGO heterostructural aerogel with enhanced and selective photocatalytic properties under visible light. *Appl. Surf. Sci.* **2017**, *396*, 1775–1782. [CrossRef]
31. Delgado, D.; Sadaoui, M.; Ludwig, W.; Méndez, W. Spatio-temporal assessment of rainfall erosivity in Ecuador based on RUSLE using satellite-based high frequency GPM-IMERG precipitation data. *Catena* **2022**, *219*, 106597. [CrossRef]
32. Shahid, M.; Rahman, K.U.; Haider, S.; Gabriel, H.F.; Khan, A.J.; Pham, Q.B.; Mohammadi, B.; Linh, N.T.; Anh, D.T. Assessing the potential and hydrological usefulness of the CHIRPS precipitation dataset over a complex topography in Pakistan. *Atmos. Res.* **2021**, *66*, 1664–1684. [CrossRef]
33. Valenzuela, R.; Garreaud, R.; Vergara, I.; Campos, D.; Viale, M.; Rondanelli, R. An extraordinary dry season precipitation event in the subtropical Andes: Drivers, impacts and predictability. *Weather Clim. Extrem.* **2022**, *37*, 100472. [CrossRef]
34. Bulovic, N.; McIntyre, N.; Johnson, F. Evaluation of imerg v05b 30-min rainfall estimates over the high-elevation tropical andes mountains. *J. Hydrometeorol.* **2020**, *21*, 2875–2892. [CrossRef]
35. Navarro, A.; García-Ortega, E.; Merino, A.; Sánchez, J.L.; Tapiador, F.J. Orographic biases in IMERG precipitation estimates in the Ebro River basin (Spain): The effects of rain gauge density and altitude. *Atmos. Res.* **2020**, *244*, 105068. [CrossRef]
36. Navarro, A.; García-Ortega, E.; Merino, A.; Sánchez, J.L.; Kummerow, C.; Tapiador, F.J. Assessment of IMERG precipitation estimates over Europe. *Remote Sens.* **2019**, *11*, 2470. [CrossRef]
37. Sarricolea, P.; Herrera-Ossandon, M.; Meseguer-Ruiz, Ó. Climatic regionalisation of continental Chile. *J. Maps* **2017**, *13*, 66–73. [CrossRef]
38. IDE Ministerio de Bienes Nacionales Chile, infraestructura de datos Geoespaciales. Available online: <http://www.ide.cl/> (accessed on 30 October 2022).
39. Scherrer, S.C.; Frei, C.; Croci-Maspoli, M.; van Geijtenbeek, D.; Hotz, C.; Appenzeller, C. Operational quality control of daily precipitation using spatio-climatological plausibility testing. *Meteorol. Zeitschrift* **2011**, *20*, 397–407. [CrossRef]
40. Estévez, J.; Llabrés-Brustenga, A.; Casas-Castillo, M.C.; García-Marín, A.P.; Kirchner, R.; Rodríguez-Solà, R. A quality control procedure for long-term series of daily precipitation data in a semiarid environment. *Theor. Appl. Climatol.* **2022**, *149*, 1029–1041. [CrossRef]
41. Dirección General de Aguas Actualización del Balance Hídrico Nacional: Resumen Ejecutivo. Santiago de Chile, Chile, 2017; 61.
42. Barrett, B.S.; Hameed, S. Seasonal variability in precipitation in central and southern Chile: Modulation by the South Pacific high. *J. Clim.* **2017**, *30*, 55–69. [CrossRef]
43. Ramadhan, R.; Yusnaini, H.; Marzuki, M.; Muharsyah, R.; Suryanto, W.; Sholihun, S.; Vonnisa, M.; Harmadi, H.; Ningsih, A.P.; Battaglia, A.; et al. Evaluation of GPM IMERG Performance Using Gauge Data over Indonesian Maritime Continent at Different Time Scales. *Remote Sens.* **2022**, *14*, 1172. [CrossRef]

44. Anagnostou, E.; Mei, Y. Using high-resolution satellite precipitation for flood frequency analysis: Case study over the Connecticut River Basin. *J. Flood Risk Manag.* **2018**, *11*, S514–S526.
45. Valenzuela, R.A.; Garreaud, R.D. Extreme daily rainfall in central-southern Chile and its relationship with low-level horizontal water vapor fluxes. *J. Hydrometeorol.* **2019**, *20*, 1829–1850. [[CrossRef](#)]
46. Li, Y.; Grimaldi, S.; Walker, J.P.; Pauwels, V.R.N. Application of remote sensing data to constrain operational rainfall-driven flood forecasting: A review. *Remote Sens.* **2016**, *8*, 456. [[CrossRef](#)]
47. Zambrano, F.; Wardlow, B.; Tadesse, T.; Lillo-Saavedra, M.; Lagos, O. Evaluating satellite-derived long-term historical precipitation datasets for drought monitoring in Chile. *Atmos. Res.* **2017**, *186*, 26–42. [[CrossRef](#)]
48. Fustos, I.; Abarca-del-Río, R.; Mardones, M.; González, L.; Araya, L.R. Rainfall-induced landslide identification using numerical modelling: A southern Chile case. *J. S. Am. Earth Sci.* **2020**, *101*, 102587. [[CrossRef](#)]
49. Schumann, G.; Kirschbaum, D.; Anderson, E.; Rashid, K. Role of Earth observation data in disaster response and recovery: From science to capacity building. In *Earth Science Satellite Applications*; Springer: Cham, Switzerland, 2016.
50. Li, Z.; Chen, M.; Gao, S.; Hong, Z.; Tang, G.; Wen, Y.; Gourley, J.J.; Hong, Y. Cross-examination of similarity, difference and deficiency of gauge, radar and satellite precipitation measuring uncertainties for extreme events using conventional metrics and multiplicative triple collocation. *Remote Sens.* **2020**, *12*, 1258. [[CrossRef](#)]
51. Nikolopoulos, E.I.; Crema, S.; Marchi, L.; Marra, F.; Guzzetti, F.; Borga, M. Impact of uncertainty in rainfall estimation on the identification of rainfall thresholds for debris flow occurrence. *Geomorphology* **2014**, *221*, 286–297. [[CrossRef](#)]
52. Tapiador, F.J.; Navarro, A.; Levizzani, V.; García-Ortega, E.; Huffman, G.J.; Kidd, C.; Kucera, P.A.; Kummerow, C.D.; Masunaga, H.; Petersen, W.A.; et al. Global precipitation measurements for validating climate models. *Atmos. Res.* **2017**, *197*, 1–20. [[CrossRef](#)]
53. Hempel, S.; Frieler, K.; Warszawski, L.; Schewe, J.; Piontek, F. A trend-preserving bias correction – The ISI-MIP approach. *Earth Syst. Dyn.* **2013**, *4*, 219–236. [[CrossRef](#)]
54. Wetterhall, F.; Pappenberger, F.; He, Y.; Freer, J.; Cloke, H.L. Conditioning model output statistics of regional climate model precipitation on circulation patterns. *Nonlinear Process. Geophys.* **2012**, *19*, 623–633. [[CrossRef](#)]

Disclaimer/Publisher’s Note: The statements, opinions and data contained in all publications are solely those of the individual author(s) and contributor(s) and not of MDPI and/or the editor(s). MDPI and/or the editor(s) disclaim responsibility for any injury to people or property resulting from any ideas, methods, instructions or products referred to in the content.